Advanced Steel Construction – Vol. 22 No. 3 (2026) 307–314
DOI:10.18057/IJASC.2026.22.3.6

UNCERTAINTY QUANTIFICATION OF STEEL TRUSS ASSEMBLY ACCURACY BASED ON ERROR PROPAGATION AND METAMODEL-BASED METHODS

Li-Hang Chen [1], Dong Liang [1, 2, *], Hai-Bin Huang [1], Li-Chao Su [2, 3] and Bo Wang [4]

[1] *School of Civil and Transportation Engineering, Hebei University of Technology, Tianjin 300401, China.*
[2] *Hebei Steel-Concrete Composite Bridge Technology Innovation Center, Xingtai Hebei 054001, China*
[3] *Xingtai Road and Bridge Construction Corporation, Xingtai Hebei 054001, China*
[4] *State Key Laboratory for Health and Safety of Bridge Structure, Wuhan 430034, China*
* *(Corresponding author: E-mail: 13622114075@139.com)*

A B S T R A C T

The manufacturing errors of steel truss members exhibit considerable randomness, potentially compromising the on-site assembly accuracy and hindering compliance with the specified assembly requirements. This paper proposes a theoretical analysis approach based on error propagation and quantifies the assembly accuracy with metamodel-based methods to address this issue. Furthermore, the reliability is taken as an indicator to ensure the assembly accuracy due to the stochasticity. First, develop error propagation and accumulation models of statically indeterminate steel trusses through structure deconstruction. Then, determine the uncertainty factor and the assembly accuracy function. Finally, compare the assembly accuracy and efficiency of the Monte Carlo simulation and approximation, simulation, and metamodel-based methods for better subsequent quantification calculation. The assembly accuracy and sensitivity analysis of two different structural steel trusses in practical engineering are conducted. The assembly accuracy results show that the assembly accuracy of the first steel truss is 1.200mm, 1.239mm, 1.053mm, and 0.988mm, and that of the second one is 1.293mm, 1.293mm, 1.088mm, and 1.010mm, all with 100% reliability. The sensitivity analysis results indicate that the angular error of the first steel truss is the most critical variable, and the rod length error of the second one plays a vital role during assembly. In addition, the theoretical research is independent of the materials and structures employed, allowing for its application to more complex structures.

A R T I C L E H I S T O R Y

Received: 25 April 2025
Revised: 4 October 2025
Accepted: 5 October 2025

K E Y W O R D S

Uncertainty quantification;
Error propagation;
Steel truss;
Assembly accuracy;
Monte Carlo simulation;
Metamodel-based methods;
Error propagation

1. Introduction

Steel truss structures are widely used in civil engineering, such as large-span bridges[1], high-rise buildings[2], stadiums[3], and airports[4]. The manufacturing errors of steel truss members exhibit considerable randomness, potentially compromising the on-site assembly accuracy and hindering compliance with the specified assembly requirements[5].

To ensure successful on-site assembly, physical pre-assembly is extensively adopted to verify the machining accuracy of members in the factory to achieve precision matching. It is used to identify quality problems in connection parts for timely resolution[6]. However, it has several shortcomings, such as high cost and a long construction period[7]. Besides, factors that influence assembly are incompletely considered. For large and spatial steel trusses, only neighboring members, instead of the whole structure, are generally physically pre-assembled[8]. Essential factors affecting assembly quality may, hence, be ignored. As a result, there are many cases in which steel trusses cannot be assembled successfully on-site, even after physical pre-assembly.

Virtual assembly, i.e., trial assembly with physical information in a digital environment, has attained widespread attention in the construction industry and has been increasingly employed to solve the above problems[9]. It has been applied in product design[10, 11], virtual construction simulation[12], assembly process simulation [13], quality checking[14], and virtual assembly systems[15]. Although virtual assembly adopts advanced measurement and digital technologies to reverse model existing members and simulate the assembly process, it still falls short of replacing physical pre-assembly in current engineering practices. The primary reason is the interferences arising from various uncertainties in the three-dimensional laser scanning, inverse modeling, and virtual assembly process, which lead to significant deviations between the virtual and practical assembly outcomes.

In practical engineering, some construction difficulties, such as complex construction conditions, high risk of construction safety, high structural linear requirements, etc., make assembly accuracy challenging to control precisely. Adjustment measures will be adopted in such cases, such as utilizing corner and elevation adjustments, longitudinal deviation adjustments, transverse deviation adjustments, and so on[16]. The main span of the steel truss girder of the Shanghai-Suzhou-Nantong Changjiang River Bridge was accurately closed after longitudinal moving, pulling back from both longitudinal and transverse directions[17]. For rapid and smooth closure of the main bridge steel girder of the Wuhu Changjiang River Rail-cum-Road Bridge with high precision, adjusting the cable forces of some stay cables, pushing and longitudinally moving girder sections on the tops of pylon piers, and adjusting temperature differences are employed[18]; During the erection of a three-main-truss steel girder of the Shanghai-Suzhou-Nantong Changjiang River Rail-cum-Road Bridge, when the diagonal rod position is inaccurate, adjustment measures such as tensile, roofing, and counter-pressure were adopted to complete the rod buttressing[19]. As proved in previously cited literature, the adjustments can effectively complete assembly for subsequent construction. However, for some geometric defects derived from manufacturing errors, it is hard to precisely decide which parts and what values to adjust because the relationship between the errors and assembly accuracy exhibits ambiguity, resulting in a cumbersome adjustment process. As a result, forced assembly generally is the final option in on-site construction[20, 21]. Thus, internal forces and deformations of statically indeterminate structures will be generated, causing more significant uncertainty and safety risks for the structural performance and the construction process. Therefore, accurately calculating assembly precision based on stochastic manufacturing errors has become an urgent and unresolved challenge during assembly.

This paper proposes a theoretical analysis approach based on error propagation and quantifies the assembly accuracy with metamodel-based methods to address the issue. Furthermore, the reliability is taken as an indicator to ensure the assembly accuracy due to the stochasticity. First, develop error propagation and accumulation models of statically indeterminate steel trusses through structure deconstruction. Then, determine the uncertainty factor and the assembly accuracy function. Finally, compare the assembly accuracy and efficiency of the Monte Carlo simulation and approximation, simulation, and metamodel-based methods for better subsequent quantification calculation. The assembly accuracy and sensitivity analysis of two different structural steel trusses in practical engineering are conducted. Assuming alterations in the shape or geometric parameters of a steel truss structure, the core methodology for analyzing and quantifying approaches used during the calculation process remains the same, which is the paper's fundamental value and key contribution. Therefore, the developed strategy is independent of the materials and structures employed, allowing for its application to more complex structures.

The subsequent sections of the paper are structured as follows: Section 2 provides a detailed description of the error propagation and accumulation modeling process of two statically indeterminate structures. Section 3 outlines the uncertainty quantification, including the uncertainty factor, the assembly accuracy function, and strategies for estimation. Taking two different structural steel trusses in practical engineering as an example, the assembly accuracy and sensitivity analysis are implemented in Section 4. Lastly, in section 5, a comprehensive summary of the key points and contributions of the paper is provided.

2. Error propagation and accumulation model

Steel truss structures, treated as statically indeterminate systems, are often analyzed through finite element simulation in structural engineering applications. However, due to the randomness of errors, repeated evaluations of the simulation process are necessary, rendering it highly time-consuming or even impractical. Error propagation and accumulation models are proposed as an alternative and more affordable method for iteratively analyzing the law of propagation and calculating assembly accuracy, considering the random error distribution. These models are developed by deconstructing statically indeterminate structures into statically determinate ones. The deconstruction assumes that the statically indeterminate structure consists of one start structure, one end structure, and n connecting structures, which can be deconstructed into a static structure by disconnecting (n-1) connecting structures.

Error modeling is divided into three steps. First, develop the coordinate system of the start, connecting, and end structures. Second, identify each member's Denavit-Hartenberg (D-H) parameters according to the coordinate systems, and calculate the coordinate transformation matrix between two neighboring coordinate systems[22]. Finally, calculate the coordinate transformation matrix between the start and the end structure coordinate systems. Accordingly, the coordinate transformation matrix between the (i-1)th and the i-th coordinate systems is shown in Eq. (1). Moreover, assuming that the 0-coordinate system is located at the start structure and the m-coordinate system is located at the end structure, the coordinate transformation matrix between the two structures is calculated by Eq. (2).

$$ {}^{i-1}_{i}T = \begin{bmatrix} \cos\theta_i & -\sin\theta_i\cos\alpha_i & \sin\theta_i\sin\alpha_i & a_i\cos\theta_i \\ \sin\theta_i & \cos\theta_i\cos\alpha_i & -\cos\theta_i\sin\alpha_i & a_i\sin\theta_i \\ 0 & \sin\alpha_i & \cos\alpha_i & d_i \\ 0 & 0 & 0 & 1 \end{bmatrix} \tag{1} $$

Where θ_i is the angle from the axis $x_{i\text{-}1}$ to x_i counterclockwise rotating in the positive direction of the $z_{i\text{-}1}$-axis; α_i is the angle from the axis $z_{i\text{-}1}$ to z_i counterclockwise rotating in the positive direction of the x_i-axis; a_i is the distance from axis $z_{i\text{-}1}$ to z_i along the positive direction of the x_i-axis; d_i is the distance from axis $x_{i\text{-}1}$ to x_i along the positive direction of the $z_{i\text{-}1}$-axis.

$$ {}^{0}_{m}T = {}^{0}_{1}T\,{}^{1}_{2}T\cdots{}^{m-1}_{m}T \tag{2} $$

Where ${}^{0}_{1}T$ is the coordinate transformation matrix between the 0-coordinate and the 1-coordinate systems; ${}^{1}_{2}T$ is that between the 1-coordinate and the 2-coordinate systems; ${}^{m-1}_{m}T$ is that between the (m-1)-coordinate s and the m-coordinate systems.

2.1. Error propagation modeling of the first statically indeterminate flat truss

Fig. 1 (a) shows the first statically indeterminate flat truss. Assume a bottom chord is the start structure, a top chord is the end structure, and assume a left web member, a diagonal web member, and a right web member are three connecting structures. Suppose the connection between the left web member and the bottom chord and between the right web member and the top chord is disconnected. In that case, the statically indeterminate flat truss is deconstructed into a static determinate one, which is shown as (b) in Fig. 1. Mark the end positions of the members at the disconnection points as A_1, A_2, B_1, and B_2, respectively. Then, four error propagation models can be developed to investigate error propagation and calculate the coordinates of the points. Since error propagation models contain rod length and angular parameters, l_1, l_2, l_3, l_4, l_5, θ_1, θ_2, θ_3, and θ_4, which are shown as (c) in Fig. 1, the three-dimensional coordinates of points A_1, A_2, B_1, and B_2, can be accurately calculated through the models, which are under the influence of the rod length and angular errors.

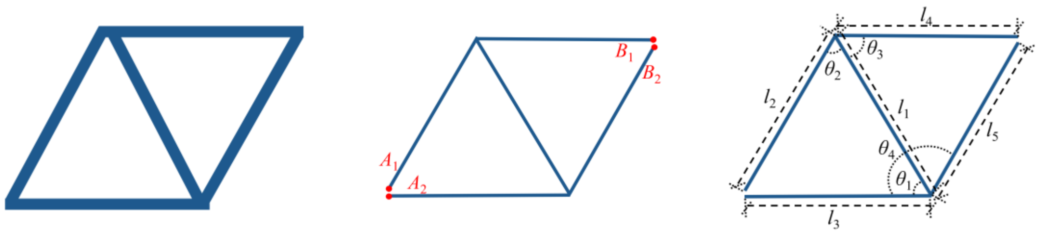

(a) A statically indeterminate flat truss

(b) A statically determinate flat truss

(c) Rod length and angular parameters

Fig. 1 The first flat truss structure

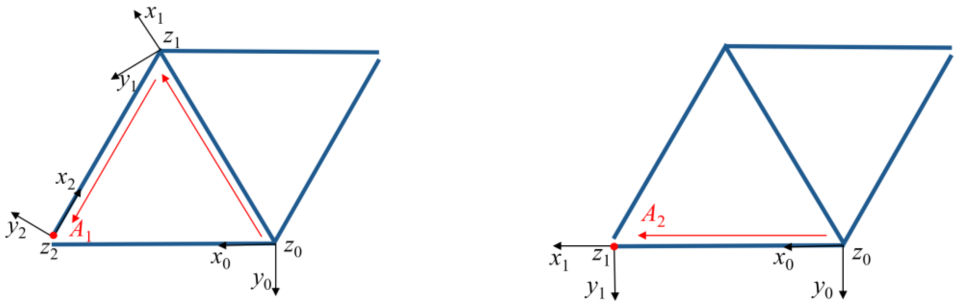

(a) Calculating A_1 coordinates

(b) Calculating A_2 coordinates

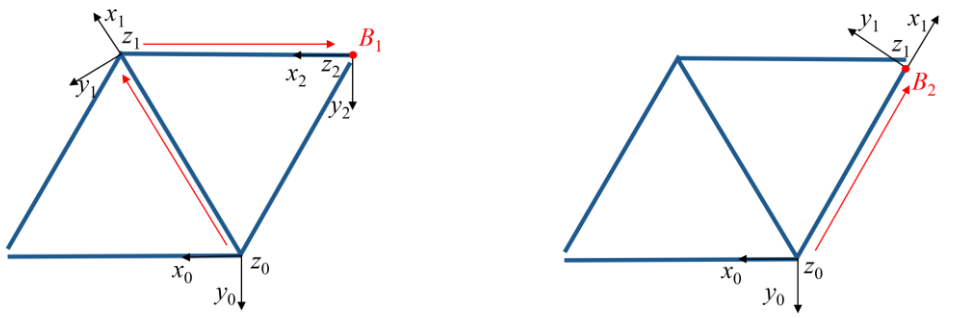

(c) Calculating B_1 coordinates

(d) Calculating B_2 coordinates

Fig. 2 Error propagation model for calculating the coordinate

As a result, the error propagation models for calculating the coordinates of A_1, A_2, B_1, and B_2 are shown separately in Fig. 2 as (a), (b), (c), and (d).

2.1.1. Error propagation model for calculating the coordinates of A_1

Assume the start and end structures of the error propagation model for calculating the coordinates of A_1 are the 0-coordinate system and the 2-coordinate system, and z_0, z_1, and z_2 are oriented perpendicular to the paper plane outward, shown as (a) in Fig. 2. The corresponding D-H parameters, $\boldsymbol{d_i}$, $\boldsymbol{a_i}$, $\boldsymbol{\alpha_i}$, and $\boldsymbol{\theta_i}$, between the 0-coordinate system and 1-coordinate systems are identified as 0, l_1, 0, and -θ_1, and that between the 1-coordinate system and 2-coordinate system are 0, -l_2, 0, and -θ_2. Substitute them in Eq. (1), and the coordinate transformation matrices between the 0-coordinate and 1-coordinate systems and the 1-coordinate and 2-coordinate systems are shown as shown in Eqs. (3) and (4).

$$ {}_1^0T=\begin{bmatrix} \cos(-\theta_1) & -\sin(-\theta_1) & 0 & l_1\cos(-\theta_1) \\ \sin(-\theta_1) & \cos(-\theta_1) & 0 & l_1\sin(-\theta_1) \\ 0 & 0 & 1 & 0 \\ 0 & 0 & 0 & 1 \end{bmatrix} \tag{3} $$

$$ {}_2^1T=\begin{bmatrix} \cos(-\theta_2) & -\sin(-\theta_2) & 0 & -l_2\cos(-\theta_2) \\ \sin(-\theta_2) & \cos(-\theta_2) & 0 & -l_2\sin(-\theta_2) \\ 0 & 0 & 1 & 0 \\ 0 & 0 & 0 & 1 \end{bmatrix} \tag{4} $$

Substitute Eqs. (3) and (4) into Eq. (2), the coordinate transformation matrix between the start and end structure coordinate systems of the error propagation model can be calculated, the result of which is shown in Eq. (5).

$$ {}_2^0T={}_1^0T\,{}_2^1T=\begin{bmatrix} \cos(\theta_1+\theta_2) & \sin(\theta_1+\theta_2) & 0 & l_1\cos\theta_1-l_2\cos(\theta_1+\theta_2) \\ -\sin(\theta_1+\theta_2) & \cos(\theta_1+\theta_2) & 0 & -l_1\sin\theta_1+l_2\sin(\theta_1+\theta_2) \\ 0 & 0 & 1 & 0 \\ 0 & 0 & 0 & 1 \end{bmatrix} \tag{5} $$

From Eq. (5), the coordinates of A_1 are shown in Eq. (6), which represents the effect of the rod length and angular parameters, l_1, l_2, θ_1, and θ_2, on the coordinates of A_1 during assembly.

$$ \begin{cases} x_{A_1}=l_1\cos\theta_1-l_2\cos(\theta_1+\theta_2) \\ y_{A_1}=-l_1\sin\theta_1+l_2\sin(\theta_1+\theta_2) \\ z_{A_1}=0 \end{cases} \tag{6} $$

2.1.2. Error propagation model for calculating the coordinates of A_2

Assume the start and end structures of the error propagation model for calculating the coordinates of A_2 are the 0-coordinate system and the 1-coordinate system, and z_0 and z_1 are oriented perpendicular to the paper plane outward, shown as (b) in Fig. 2. The corresponding D-H parameters, $\boldsymbol{d_i}$, $\boldsymbol{a_i}$, $\boldsymbol{\alpha_i}$, and $\boldsymbol{\theta_i}$, between the 0-coordinate system and 1-coordinate system are identified as 0, l_3, 0, and 0. Substitute them in Eq. (1), and the coordinate transformation matrix between the 0-coordinate system and 1-coordinate system is shown in Eq. (7).

$$ {}_1^0T=\begin{bmatrix} 1 & 0 & 0 & l_3 \\ 0 & 1 & 0 & 0 \\ 0 & 0 & 1 & 0 \\ 0 & 0 & 0 & 1 \end{bmatrix} \tag{7} $$

From Eq. (7), the coordinates of A_2 are shown in Eq. (8), which represents the effect of the rod length parameter, l_3, on the coordinates of A_2 during assembly.

$$ \begin{cases} x_{A_2}=l_3 \\ y_{A_2}=0 \\ z_{A_2}=0 \end{cases} \tag{8} $$

2.1.3. Error propagation model for calculating the coordinates of B_1

Assume the start and end structures of the error propagation model for calculating the coordinates of B_1 is the 0-coordinate system and the 2-coordinate system, and z_0, z_1, and z_2 are oriented perpendicular to the paper plane outward, shown as (c) in Fig. 2. The corresponding D-H parameters, $\boldsymbol{d_i}$, $\boldsymbol{a_i}$, $\boldsymbol{\alpha_i}$, and $\boldsymbol{\theta_i}$, between the 0-coordinate system and 1-coordinate system are identified as 0, l_1, 0, and -θ_1, and that between the 1-coordinate system and 2-coordinate system are 0, -l_4, 0, and θ_3. Substitute them in Eq. (1), and the coordinate transformation matrices between the 0-coordinate system and 1-coordinate system, as well as the 1-coordinate system and 2-coordinate system, are calculated as shown in Eqs. (9) and (10).

$$ {}_1^0T=\begin{bmatrix} \cos(-\theta_1) & -\sin(-\theta_1) & 0 & l_1\cos(-\theta_1) \\ \sin(-\theta_1) & \cos(-\theta_1) & 0 & l_1\sin(-\theta_1) \\ 0 & 0 & 1 & 0 \\ 0 & 0 & 0 & 1 \end{bmatrix} \tag{9} $$

$$ {}_2^1T=\begin{bmatrix} \cos\theta_3 & -\sin\theta_3 & 0 & -l_4\cos\theta_3 \\ \sin\theta_3 & \cos\theta_3 & 0 & -l_4\sin\theta_3 \\ 0 & 0 & 1 & 0 \\ 0 & 0 & 0 & 1 \end{bmatrix} \tag{10} $$

Substitute Eqs. (9) and (10) into Eq. (2), the coordinate transformation matrix between the start and end structure coordinate systems of the error propagation model can be calculated, the result of which is shown in Eq. (11).

$$ {}_2^0T={}_1^0T\,{}_2^1T=\begin{bmatrix} \cos(\theta_1\text{-}\theta_3) & \sin(\theta_1\text{-}\theta_3) & 0 & l_1\cos\theta_1\text{-}l_4\cos(\theta_1\text{-}\theta_3) \\ -\sin(\theta_1\text{-}\theta_3) & \cos(\theta_1\text{-}\theta_3) & 0 & -l_1\sin\theta_1+l_4\sin(\theta_1\text{-}\theta_3) \\ 0 & 0 & 1 & 0 \\ 0 & 0 & 0 & 1 \end{bmatrix} \tag{11} $$

From Eq. (11), the coordinates of B_1 are shown in Eq. (12), which represents the effect of the rod length and angular parameters, l_1, l_4, θ_1, and θ_3, on the coordinates of B_1 during assembly.

$$ \begin{cases} x_{B_1}=l_1\cos\theta_1\text{-}l_4\cos(\theta_1\text{-}\theta_3) \\ y_{B_1}=-l_1\sin\theta_1+l_4\sin(\theta_1\text{-}\theta_3) \\ z_{B_1}=0 \end{cases} \tag{12} $$

2.1.4. Error propagation model for calculating the coordinates of B_2

Assume the start and end structures of the error propagation model for calculating the coordinates of B_2 are the 0-coordinate system and the 1-coordinate system, and z_0 and z_1 are oriented perpendicular to the paper plane outward, shown as (d) in Fig. 2. The corresponding D-H parameters, $\boldsymbol{d_i}$, $\boldsymbol{a_i}$, $\boldsymbol{\alpha_i}$, and $\boldsymbol{\theta_i}$, between the 0-coordinate system and 1-coordinate system are identified as 0, l_5, 0, and -θ_4. Substitute them in Eq. (1), and the coordinate transformation matrix between the 0-coordinate system and 1-coordinate system is shown in Eq. (13).

$$ {}_1^0T=\begin{bmatrix} \cos(-\theta_4) & -\sin(-\theta_4) & 0 & l_5\cos(-\theta_4) \\ \sin(-\theta_4) & \cos(-\theta_4) & 0 & l_5\sin(-\theta_4) \\ 0 & 0 & 1 & 0 \\ 0 & 0 & 0 & 1 \end{bmatrix} \tag{13} $$

From Eq. (13), the coordinates of B_2 are shown in Eq. (14), which represents the effect of the rod length and angular parameters, l_5 and θ_4, on the coordinates of B_2 during assembly.

$$ \begin{cases} x_{B_2}=l_5\cos\theta_4 \\ y_{B_2}=-l_5\sin\theta_4 \\ z_{B_2}=0 \end{cases} \tag{14} $$

2.2. Error propagation modeling of the second statically indeterminate flat truss

Fig. 3 (a) shows a different statically indeterminate flat truss structure.

Fig. 4 shows the error propagation models for calculating the points A'_1, A'_2, B'_1, and B'_2 coordinates. The coordinate representation and subsequent calculation are the same as those in Section 2.1.

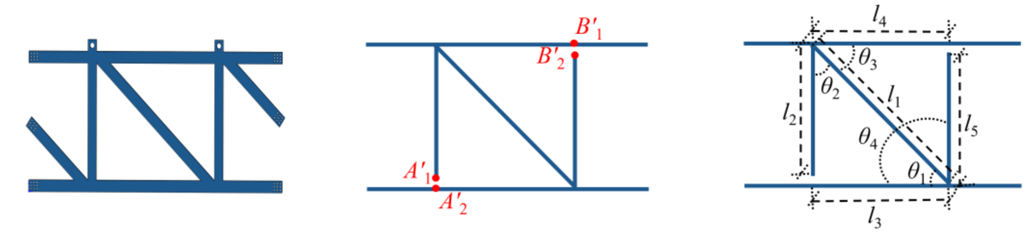

(a) Another statically indeterminate flat truss

(b) Corresponding statically determinate flat truss

(c) Rod length and angular parameters

Fig. 3 The second flat truss structure

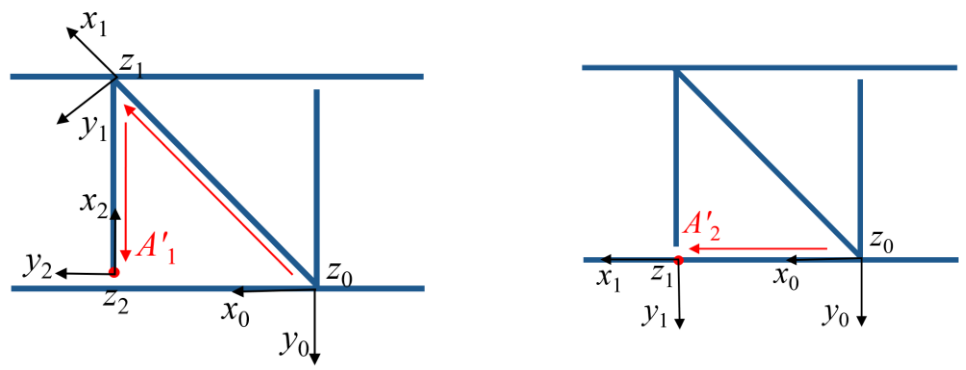

Calculating A'_1 coordinates

Calculating A'_2 coordinates

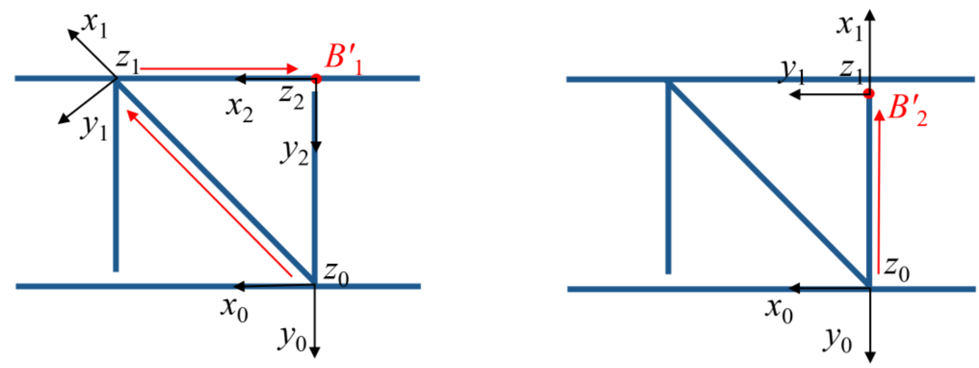

Calculating B'_1 coordinates

Calculating B'_2 coordinates

Fig. 4 Error propagation model for calculating coordinates

3. Uncertainty quantification

3.1. Uncertainty factor

All uncertainty factors affecting assembly accuracy during the on-site assembly are represented as rod length and angular errors in the error propagation and accumulation models. Manufacturing error is one dominant factor causing rod length error, and ambient temperature variance is the other. The i-th rod length l_i during assembly is shown in Eq. (15).

$$l_i=\left(l_{di}+l_{ei}\right)\times\left(1+\alpha\times\Delta T\right) \tag{15}$$

Where l_{di} is the designed value, mm; l_{ei} is a manufacturing error, mm; α is the linear expansion coefficient, 1/℃; ΔT is the ambient temperature variance, ℃.

The angular error also resulted from the manual connecting process. The i-th angle θ_i during assembly is shown in Eq. (16). Suppose a rod length is l_m, and the permitted deviation diameter of which is d, its maximum angular error range is $\pm arctan(d/l_m)$.

$$\theta_i=\theta_{di}+\theta_{ei} \tag{16}$$

Where θ_{di} is the designed value, °; θ_{ei} is the error value, °.

3.2. Assembly accuracy function

Eq. (17) shows the assembly deviation d_A between A_1 and A_2 and d_B between B_1 and B_2 of steel trusses in Sections 2.1 and 2.2. If any d_A or d_B is greater than the designed value of assembly accuracy, the assembly cannot be completed; conversely, it can be completed.

$$d_A=\sqrt{\left\{\left[l_1\cos\theta_1-l_2\cos\left(\theta_1+\theta_2\right)\right]-l_3\right\}^2+\left[-l_1\sin\theta_1+l_2\sin\left(\theta_1+\theta_2\right)\right]^2} \tag{17}$$

$$d_B=\sqrt{\left\{\left[l_1\cos\theta_1\text{-}l_4\cos\left(\theta_1\text{-}\theta_3\right)\right]-l_5\cos\theta_4\right\}^2+\left\{\left[-l_1\sin\theta_1+l_4\sin\left(\theta_1\text{-}\theta_3\right)\right]-\left(-l_5\sin\theta_4\right)\right\}^2}$$

Where l_1, l_2, and l_5 are the diagonal, left, and right web members of the flat truss; l_4 and l_3 are the top and bottom chords of the flat truss; θ_1, θ_2, θ_3, and θ_4 are the angles between the diagonal web member and the bottom chord, between the diagonal web member and the left web member, between the diagonal web member and the top chord, and between the bottom chord and the right web member.

3.3. Strategies for estimation

In the presence of uncertainties regarding the system's physical properties, the structure may operate outside its nominal range. Given all uncertainty factors, the uncertainty analysis aims to quantitatively assess the probability that the structural assembly accuracy on-site satisfies the designed specifications during the assembly process. The Monte Carlo simulation[23] is generally adopted to estimate probability. According to the law of large numbers in statistics, if the samples are large enough, the calculated results of the Monte Carlo simulation will gradually converge to the actual value. Therefore, the paper's sample size is 1e6 [24, 25]. However, it is often time-consuming because it requires repeated evaluations of the computational model describing the system's behavior.

The approximation, simulation, and metamodel-based adaptive methods are used for calculation and comparison to improve the calculation efficiency. The approximation methods, including First Order Reliability Method (FORM)[26, 27] and Second Order Reliability Method (SORM)[28, 29], are based on approximating the limit-state function locally at a reference point. The simulation methods, such as Importance Sampling (IS)[30, 31] and Subset Simulation (SS)[32], are based on sampling the joint distribution of the state variables and using sample-based estimates of the integral. The metamodel-based adaptive methods, evidenced by Adaptive Kriging Monte Carlo Simulation (AK-MCS)[33, 34] and Bayesian Line Sampling (BLS)[35, 36], are based on iteratively building surrogate models that approximate the limit-state function in the direct vicinity of the limit-state surface.

4. Case study

4.1. Uncertainty quantification of the first flat truss

The designed geometric parameters, l_1, l_2, l_3, l_4, l_5, θ_1, θ_2, θ_3, θ_4, are 6042mm, 6042mm, 5000mm, 5000mm, 6042mm, 65.556°, 48.888°, 65.556°, and 114.444°, separately. The manufacturing error of the rod length is ±1mm. The permitted deviation diameter of bolts is 0.3mm, which aligns with *Tolerances for fasteners—Bolts, screws, studs, and nuts (GB/T 3103.1-2002)*[37]. Referring to the law of calculating the angular error range in section 3.1, the angular error range of he left, right, and diagonal web members is ±0.0028°.

After being prefabricated at the factory, steel trusses were transported to the actual construction site. The distance between the two places and the difference in altitude resulted in a significant change in ambient temperature during the manufacturing and assembly. The ambient temperature of the factory is a high temperature of 42°C and a low of -6°C, and that of the construction site is a high temperature of 39°C and a low of -5°C. Therefore, the cooling and warming ranges between the two places are 3 to 47°C and 1 to 45°C. Assuming the rod length and angular error follow a truncated normal distribution[38], different error groups of the flat truss are shown in Table 1. Groups 1 and 2 are set for calculating the assembly accuracy and corresponding reliability between A_1 and A_2, and 3 and 4 between B_1 and B_2.

Table 1
Different error groups of the flat truss

Error group		1	2	3	4
Ambient temperature variance range		Warming：1~45°C	Cooling: 3~47°C	Warming: 1~45°C	Cooling：3~47°C
Rod length error	Value	±1mm		±1mm	
	Distribution type	Truncated normal distribution		Truncated normal distribution	
	Mean value	0		0	
	Standard deviation	0.333		0.333	
	Truncation point	[-1, 1]		[-1, 1]	
Angular error of the left and right web members	Value	/		±0.0028°	
	Distribution type	/		Truncated normal distribution	
	Mean value	/		0	
	Standard deviation	/		0.000933	
	Truncation point	/		[-0.0028, 0.0028]	
Angular error of the diagonal web member	Value	±0.0028°		±0.0028°	
	Distribution type	Truncated normal distribution		Truncated normal distribution	
	Mean value	0		0	
	Standard deviation	0.000933		0.000933	
	Truncation point	[-0.0028, 0.0028]		[-0.0028, 0.0028]	

Fig. 5(a) displays the 1e6 sample points obtained through the Monte Carlo simulation. Fig. 5(b) presents a composite plot illustrating the distribution characteristics of response values, integrating a histogram (grey background), probability density function (PDF, blue curve), and cumulative distribution function (CDF, red curve). Besides, the left Y-axis labelled probability density quantifies the density of the response values within specific intervals, and the right Y-axis labelled cumulative probability indicates the cumulative probability of response values falling below a given threshold, ranging from 0 to 1. The histogram illustrates the frequency distribution of the response values. The PDF provides a smoothed estimate of the probability density across the continuous range of response values, serving as a theoretical fit to the histogram. The CDF shows the cumulative probability of response values up to a specific point, capturing the overall trend of the distribution. The results show that the assembly accuracy corresponding to a cumulative probability density of 100% is 1.2 mm.

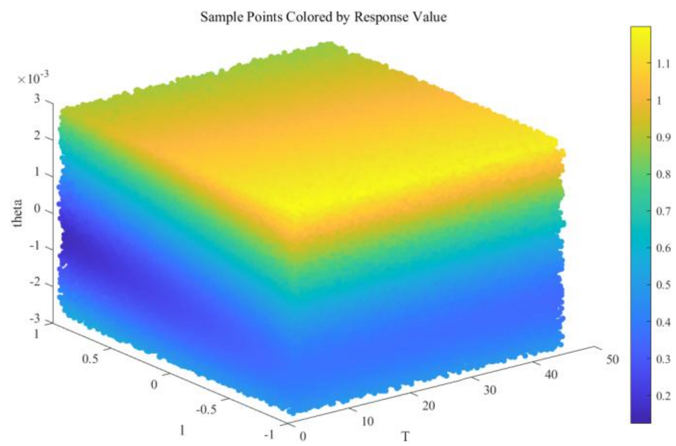

(a) Sample points

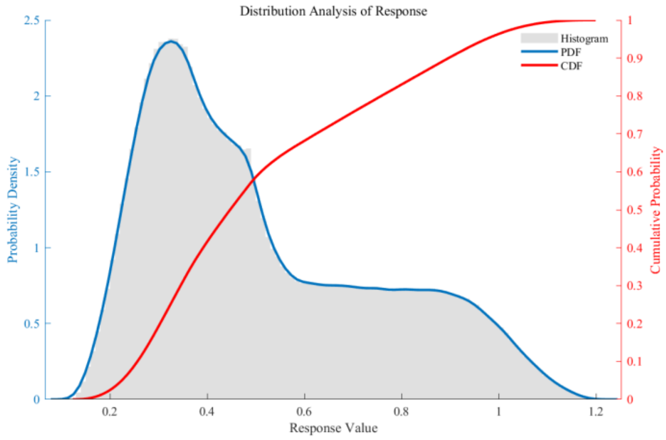

(b) Distribution analysis

Fig. 5 Sample points and response value using the Monte Carlo simulation

Take the assembly accuracy of MCS as the datum, the FORM, SORM, IS, SS, AK-MCS, and BLS are separately used for better calculation efficiency. Table 2 shows the results of different approaches for Group 1. The $\hat{P}_f$ represents the cumulative probability, and ζ indicates the percentage of relative error of assembly accuracy estimated by the other methods with the datum value, which is shown in Eq. (18). The value's magnitude indicates the technique's estimation accuracy relative to the datum value. Specifically, a smaller value denotes a closer agreement between the estimated result and the datum value, thereby implying higher computational precision. In contrast, a larger value suggests a greater discrepancy between the method's estimate and the datum value, indicating a lower level of accuracy.

$$\zeta = \left| \frac{P_f - P_{f,MCS}}{P_{f,MCS}} \right| \times 100\% \tag{18}$$

Where P_f is the assembly accuracy of different methods; $P_{f,MCS}$ is the datum assembly accuracy of the MCS.

Among all methods, the SS, based on iteratively solving and combining a sequence of conditional reliability analyses utilizing Markov Chain Monte Carlo (MCMC) simulation, has the same assembly accuracy as the MCS with fewer sample points, reduced by a factor of 10. Besides, using a Bayesian active learning framework in combination with line sampling, the BLS has only 0.083% of ζ with sample points of 130, demonstrating exceptionally high computational efficiency and extremely low error. Fig. 6 shows the probability density and cumulative distribution of SS and BLS. It is concluded that SS has the highest accuracy, and BLS maintains exceptionally high accuracy with an extremely low sample size. The BLS perfectly balances sample size and accuracy, ideally suited for high-cost or real-time analysis scenarios. Therefore, it is adopted to calculate the assembly accuracy from Groups 2 to 4, which are 1.239mm, 1.053mm, and 0.988mm, all with 100% reliability.

Table 2
Different approaches for Group 1

Error group	Method	Sample point	Assembly accuracy (mm)	$\hat{P}_f$ (%)	ζ(%)
Datum	MCS	1×10^6	1.200	100	0
Approximation method	FORM	1×10^6	1.198	100	0.167
	SORM	1×10^6	1.204	100	0.333
Simulation method	IS	1×10^3	1.207	100	0.583
	SS	1×10^5	1.200	100	0
Metamodel-based method	AK-MCS	1×10^5	1.195	100	0.417
	BLS	130	1.201	100	0.083

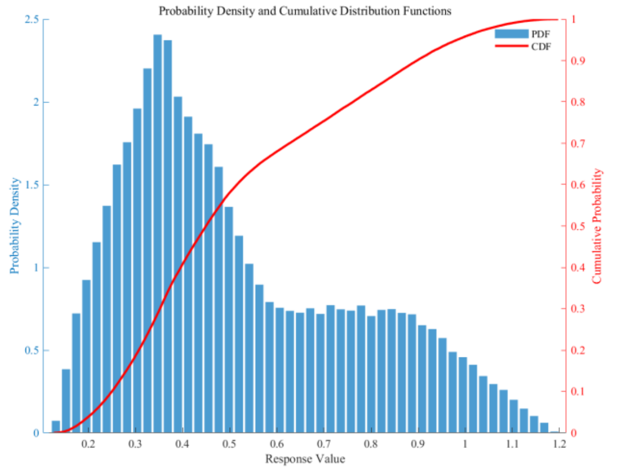

(a) Probability density and cumulative distribution functions of Subset Simulation

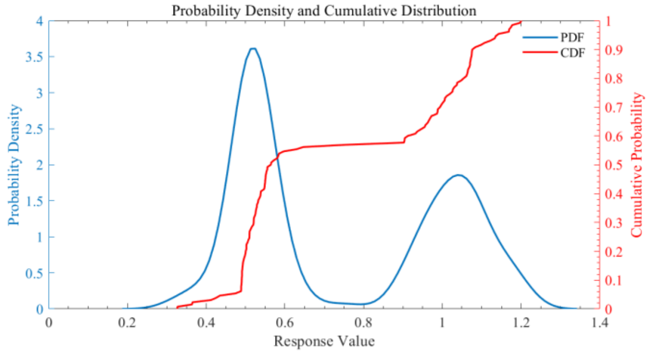

(b) Probability density and cumulative distribution of Bayesian Line Sampling

Fig. 6 Probability density and cumulative distribution

Table 3
Different error groups of the spatial truss

Error group		1	2	3	4
Ambient temperature variance range		Warming: 0~46℃	Cooling: 2~48℃	Warming: 0~46℃	Cooling: 2~48℃
Rod length error	Value	±1.5mm		±1.5mm	
	Distribution type	Truncated normal distribution		Truncated normal distribution	
	Mean value	0		0	
	Standard deviation	0.5		0.5	
	Truncation point	[-1.5, 1.5]		[-1.5, 1.5]	
Angular error of the left and right web members	Value	/		±0.001°	
	Distribution type	/		Truncated normal distribution	
	Mean value	/		0	
	Standard deviation	/		0.000333	
	Truncation point	/		[-0.001, 0.001]	

Angular error of the diagonal web member	Value	±0.0008°		±0.0008°	
	Distribution type	Truncated normal distribution		Truncated normal distribution	
	Mean value	0		0	
	Standard deviation	0.000267		0.000267	
	Truncation point	[-0.0008, 0.0008]		[-0.0008, 0.0008]	
Assembly accuracy		1.293mm	1.293mm	1.088mm	1.010mm
Reliability		100%		100%	

4.2. Uncertainty quantification of the second flat truss

Similarly, the designed values of rod length and angular parameters, l_1, l_2, l_3, l_4, l_5, θ_1, θ_2, θ_3, θ_4, are 20887mm, 15500mm, 14000mm, 14000mm, 15500mm, 47.911°, 42.089°, 47.911°, and 90°, separately. The rod length manufacturing error range is ±1.5mm. The angular error range of left and right web members is ±0.001°, and that of the diagonal web member is ±0.0008°. The cooling and warming ranges are 2 to 48°C and 0 to 46°C.

Table 3 shows different error groups. Groups 1 and 2 are set for calculating the assembly accuracy and corresponding reliability between A'_1 and A'_2, and Groups 3 and 4 between B'_1 and B'_2. The results of using BLS to calculate the assembly accuracy are shown in Table 3, and they are all 100% reliable.

4.3. Sensitivity analysis

Let $M(x)$ be an error propagation model, depending on input uncertainty factors, including ambient temperature, length error, and angular error, described by a random vector X. The aim of sensitivity analysis is to investigate how the uncertainty of assembly accuracy is assigned to each input variables X, through $M(x)$. The Sobol' indices[39], predicated on expanding the computational model into summands of increasing dimensionality, serve as reference indices. The Sobol' decomposition is defined in Eq. (19).

$$f\left(x_1,\cdots,x_M\right)=f_0+\sum_{i=1}^{M} f_i\left(x_i\right)+\sum_{1\le i\le j\le M} f_{ij}\left(x_i,x_j\right)+\cdots+f_{1,2,\cdots,M}\left(x_1,\cdots,x_M\right) \tag{19}$$

The relative contribution of each group of variables $\{x_i, \ldots, x_{is}\}$ to the total variance is represented in Eq. (20). The index concerning one input variable X_i is called the first-order Sobol' index and describes the effect of X_i alone. The multiple-term indices, e.g., S_{ij}, $i \neq j$, are referred to as higher-order Sobol' indices, which are interaction indices that account for the effects of the interactions of X_i and X_j that cannot be decomposed into the contributions of those variables separately[40].

$$S_{i1,\cdots,is}=\frac{D_{i1,\cdots,is}}{D} \tag{20}$$

Fig. 7 shows the sensitivity analysis results. For the first steel truss in Section 2.1, the First-order Sobol' indices of ambient temperature, length error, and angular error are 0.010755, 0.100913, and 0.893942, as well as the Total-order Sobol' indices are 0.004019, 0.102175, and 0.895793, indicating that the angular error is the most critical variable comparing with ambient temperature and rod length errors. Therefore, focusing on calibrating assembly angles with higher precision can elevate assembly accuracy in such structural practical engineering. Similarly, for the second steel truss in Section 2.2, the First-order Sobol's indices of ambient temperature, length error, and angular error are -0.003955, 0.807207, and 0.177581, and the Total-order Sobol's indices are 0.000007, 0.824145, and 0.192590, representing that the rod length error plays a vital role during assembly.

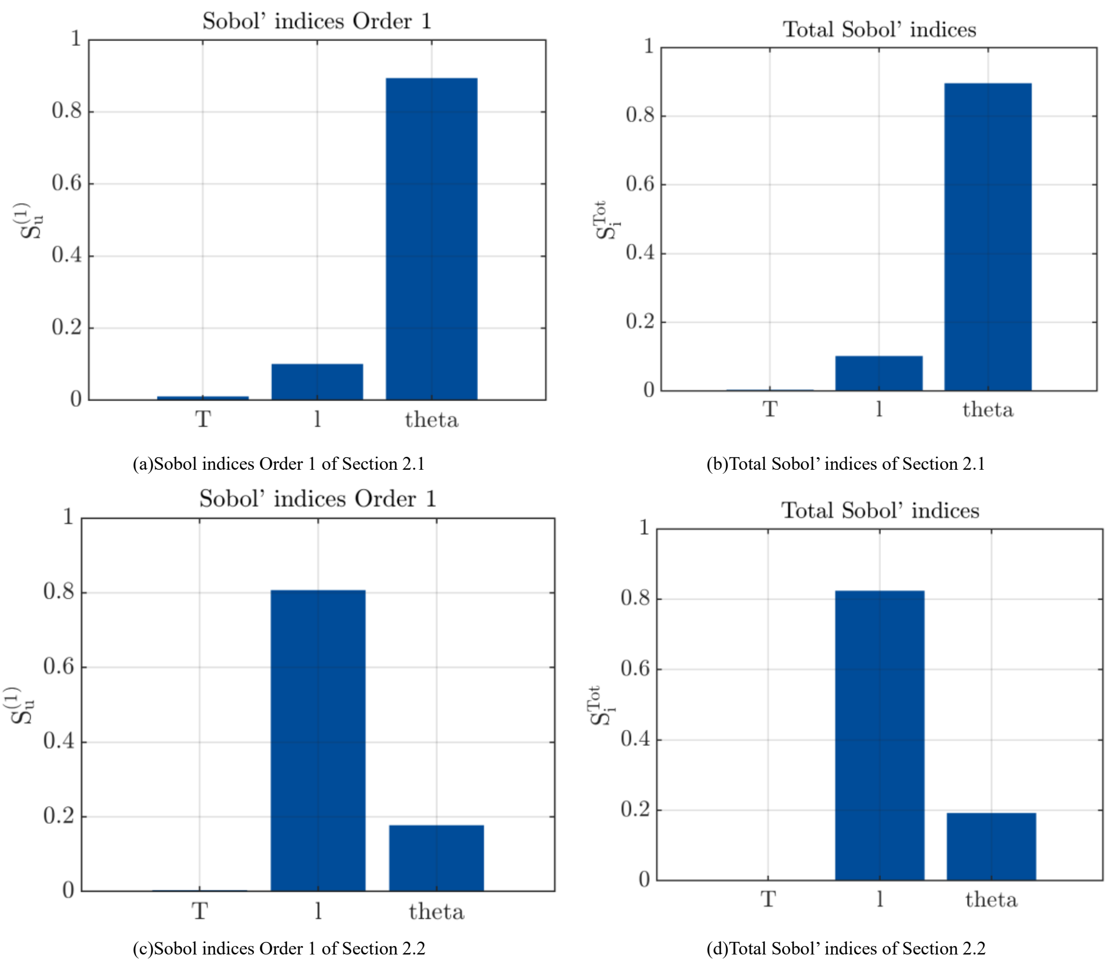

(a)Sobol indices Order 1 of Section 2.1

(b)Total Sobol' indices of Section 2.1

(c)Sobol indices Order 1 of Section 2.2

(d)Total Sobol' indices of Section 2.2

Fig. 7 Sensitivity analysis results

5. Conclusion

This paper aims to quantify the on-site assembly accuracy of members exhibiting random manufacturing errors. The key findings are listed below.

(1) This paper proposes a theoretical analysis approach based on error propagation and quantifies the assembly accuracy with metamodel-based methods. Due to stochasticity, its reliability is used as an indicator to ensure assembly accuracy. The research is independent of the materials and structures employed, allowing for its application to more complex structures.

(2) The error propagation and accumulation models of statically indeterminate structures are developed through structure deconstruction, which has broad applicability in investigating errors with no limitation on various structural figures and geometric dimensions.

(3) Based on the assembly accuracy of MCS, approximation methods including FORM and SORM, simulation methods such as IS and SS, and metamodel-based adaptive methods incorporating AK-MCS and BLS, are used for better calculation efficiency. The results show that SS has the highest accuracy and BLS perfectly balances sample size and accuracy.

(4) The assembly accuracy of the first steel truss is 1.200mm, 1.239mm, 1.053mm, and 0.988mm, and that of the second one is 1.293mm, 1.293mm, 1.088mm, and 1.010mm, all with 100% reliability. The sensitivity analysis results indicate that the angular error of the first steel truss is the most critical variable and the rod length error of the second one plays a vital role during assembly.

Declaration of competing interest

The authors declare that they have no known competing financial interests or personal relationships that could have appeared to influence the work reported in this paper.

Data Availability

Data will be made available on request.

Acknowledgements

The authors acknowledge the financial support from the National Natural Science Foundation of China (No. 52478310).

Reference

[1] B. Shangguan, H. Y. Hu, P. H. Ning and Q. T. Su. "Mingzhuwan Bridge: the largest span three-main-truss steel arch bridge." Structural Engineering International, 33(1), 89-95, 2023
[2] X. K. Zou, Y. Zhang, Y. P. Liu, L. C. Shi and D. Kan. "Design and construction of high-performance long-span steel transfer twin trusses applied in one hospital building in Hong Kong." Buildings, 13(3), 2023
[3] Y. FENG, Y. ZHANG, L. WANG, X. XIANG and T. QIU. "Structural analysis of steel structure of a 60,000-seats stadium." Journal, 2023(Issue), 1-12, 2023
[4] G. Cheng, W. Zheng, H. Chen, C. Zhu and Y. Li. "Key technology of steel roof manufacturing of Hangzhou Xiaoshan International Airport T4 terminal building." Building Structure, 51(23), 34-37, 2021
[5] J. Lu and W. Chen. "Structural design and manufacturing length errors analyses of crossed spoke cable-truss structure." Advances in Structural Engineering, 26(7), 1260-1275, 2023
[6] G. Cheng, J. Liu, N. Cui, H. Hu, C. Xu and J. Tang. "Virtual trial assembly of large steel members with bolted connections based on point cloud data." Automation in Construction, 151(104866, 2023
[7] Y. Zhou, D. G. Han, K. X. Hu, G. C. Qin, Z. F. Xiang, C. L. Ying, L. D. Zhao and X. Y. Hu. "Accurate virtual trial assembly method of prefabricated steel components using terrestrial laser scanning." Advances in Civil Engineering, 2021(2021
[8] T. Lu, S. Wang, A. Wang, L. Luo, W. Li and M. Wang. "Research and application of key technology in construction of steel structure of super-high and large-span heavy duty globular corridor." Journal, 790-795, 2021
[9] M. Guo, S. Guo, Q. Meng, M. Liu, J. Wang, C. Cui and X. Zhang. "Intelligent virtual trial assembly of prefabricated frame structures for large and complex construction scenes." Automation in Construction, 172(106047, 2025
[10] J. Madrid, S. Lorin, R. Söderberg, P. Hammersberg, K. Wärmefjord and J. Lööf. "A virtual design of experiments method to evaluate the effect of design and welding parameters on weld quality in aerospace applications." Aerospace, 6(6), 74, 2019
[11] Y. Yi, Y. Yan, X. Liu, Z. Ni, J. Feng and J. Liu. "Digital twin-based smart assembly process design and application framework for complex products and its case study." Journal of Manufacturing Systems, 58(94-107, 2021
[12] Liu C, Liu Y and Chen Y. "A state-of-the-practice review of three-dimensional laser scanning technology for tunnel distress monitoring." Journal of Performance of Constructed Facilities, 37(2), 03123001, 2023
[13] L. Xiaoguang and P. Yongjie. "Application of virtual pre-assembly technology for steel truss girder." Railway Engineering, 60(01), 1-6, 2020
[14] Guo J, Wang Q and P. J. H. "Geometric quality inspection of prefabricated MEP modules with 3D laser scanning." Automation in Construction, 111(103053, 2020
[15] D. Hongwang, W. Xiong, W. Haitao and W. Zuwen. "Physical modeling and geometry configuration simulation for flexible cable in a virtual assembly system." Assembly Automation, 40(6), 905-915, 2020
[16] Z. Jianjin. "Key technology for Wutong Minjiang ridge closure of Chengdu-Guiyang high speed railway." Construction Technology, 46(20), 27-30, 2017
[17] L. Jun-tang. "Integral manufacturing and erection techniques for steel truss girder of main navigational channel bridge of Shanghai-Suzhou-Nantong Changjiang River Bridge." Bridge Construction, 50(05), 10-15, 2020
[18] l. Ailin and L. Xu. "Key erection techniques for main bridge steel girder of Wuhu Changjiang River Rail-cum-Road Bridge on Shangqiu-Hefei-Hangzhou Railway." Bridge Construction, 50(01), 1-6, 2020
[19] C. Tao. "Key erection techniques for two-panel large segments of three-main-truss steel girder." Bridge Construction, 50(06), 8-13, 2020
[20] W. Haibin. "Erection techniques for continuous steel truss girder of Huanghe River Rail-cum-Road Bridge of Zhengzhou-Jinan High-Speed Railway." Bridge Construction, 52(05), 8-13, 2022
[21] X. Chuanchang. "Stochastic finite element method for structural of continous beam bridge during the construction process." Journal, 2009
[22] M. W. Spong, S. Hutchinson and M. Vidyasagar. "Robot modeling and control." Journal, 2020
[23] S. Raychaudhuri. "Introduction to Monte Carlo simulation." Journal, 91-100, 2008
[24] L. Hong, H. Li and J. Fu. "A novel surrogate-model based active learning method for structural reliability analysis." Computer Methods in Applied Mechanics and Engineering, 394(114835, 2022
[25] L. Hong, B. Shang, S. Li, H. Li and J. Cheng. "Portfolio allocation strategy for active learning Kriging-based structural reliability analysis." Computer Methods in Applied Mechanics and Engineering, 412(116066, 2023
[26] M. Behtash and M. Alexander-Ramos. "A Comparative Study Between the Generalized Polynomial Chaos Expansion-and First-Order Reliability Method-Based Formulations of Simulation-Based Control Co-Design." Journal of Mechanical Design, 146(8), 2024
[27] H. R. Maier, B. J. Lence, B. A. Tolson and R. O. Foschi. "First-order reliability method for estimating reliability, vulnerability, and resilience." Water Resources Research, 37(3), 779-790, 2001
[28] J. Zhang and X. Du. "A second-order reliability method with first-order efficiency." Journal of Mechanical Design, 10(132), 101006, 2010
[29] Z. Hu, R. Mansour, M. Olsson and X. Du. "Second-order reliability methods: a review and comparative study." Structural and Multidisciplinary Optimization, 64(3233–3263, 2021
[30] A. Tabandeh, G. F. Jia and P. Gardoni. "A review and assessment of importance sampling methods for reliability analysis." Structural Safety, 97(2022
[31] S. T. Tokdar and R. E. Kass. "Importance sampling: a review." Wiley Interdisciplinary Reviews: Computational Statistics, 2(1), 54-60, 2010
[32] S.-K. Au and J. L. Beck. "Estimation of small failure probabilities in high dimensions by subset simulation." Probabilistic engineering mechanics, 16(4), 263-277, 2001
[33] L. Puppo, N. Pedroni, A. Bersano, F. Di Maio, C. Bertani, E. Zio and Design. "Failure identification in a nuclear passive safety system by Monte Carlo simulation with adaptive Kriging." Nuclear Engineering, 380(111308, 2021
[34] B. Echard, N. Gayton and M. Lemaire. "AK-MCS: an active learning reliability method combining Kriging and Monte Carlo simulation." Structural safety, 33(2), 145-154, 2011
[35] C. Dang, M. A. Valdebenito, P. Wei, J. Song, M. Beer and S. Safety. "Bayesian active learning line sampling with log-normal process for rare-event probability estimation." Reliability Engineering, 246(110053, 2024
[36] C. Dang, M. A. Valdebenito, M. G. R. Faes, J. Song, P. Wei and M. Beer. "Structural reliability analysis by line sampling: A Bayesian active learning treatment." Structural Safety, 104(102351, 2023
[37] Standard. "Tolerances for fasteners—bolts, screws, studs and nuts (GB/T 3103.1-2002)." Journal, 2002
[38] Y. Cheng, X. Zhuang and T. Yu. "Time-dependent reliability analysis of planar mechanisms considering truncated random variables and joint clearances." Probabilistic Engineering Mechanics, 75(103552, 2024
[39] S. I. M. "Sensitivity estimates for nonlinear mathematical models." Mathematical Modelling and Computational Experiments, 1(1), 112-118, 1993
[40] S. Marelli, C. Lamas, K. Konakli, C. Mylonas, P. Wiederkehr and B. Sudret. "UQLab user manual– Sensitivity analysis." Journal, Report UQLab-V2.1-106(Issue), 2024